BNL-229876-2026-TECH

CA/AP/751

Measurement of the Emittance for the CeC Project

I. Pinayev

June 2026

Collider Accelerator Department

Brookhaven National Laboratory

U.S. Department of Energy

USDOE Office of Science (SC), Nuclear Physics (NP)

DISCLAIMER

Measurement of the Emittance for the CeC Project

I. Pinayev

Coherent Electron Cooling (CeC) experiment was carried out at RHIC [1]. It required small emittance of 10-15 MeV electron beam with high peak current. In most cases the emittance was measured by either quadrupole or solenoid scan. For a low-energy beam with high peak current the measurements are affected by space charge forces. To overcome these difficulties the pepper-pot [2,3] or slit scan [4] can be used.

Not only small emittance is required for CeC based on the plasma-cascade instability but the beam uniformity in the core. The slice emittance can be measured with slit when the beam is streaked with transverse deflecting cavity [5, 6]. Quadrupole scan can be utilized for this purpose as well [7].

Experimental Set Up

The general description of the CeC diagnostics can be found in [8]. The low energy beam from the gun is transported through low-energy beamline (LEBT) to the linac where it is accelerated to the final energy. The transverse focusing in LEBT is provided by six solenoids which have individual bipolar power supplies. The beam cross section can be observed at two profile monitors. The first profile monitor YAG1 is located 0.64 meters downstream of the second solenoid LEBT1. The second profile monitor YAG2 is placed 0.77 meters after the fourth solenoid LEBT3. In front of the YAG2 there is a pepper pot mask for emittance measurement. The distance between the pepper pot and the profile monitor is 0.34 meters. Between the gun and LEBT1 solenoids the integrating current transformer is placed. The cameras and other diagnostics equipment are triggered from the common timing system. The trigger delays can be individually adjusted.

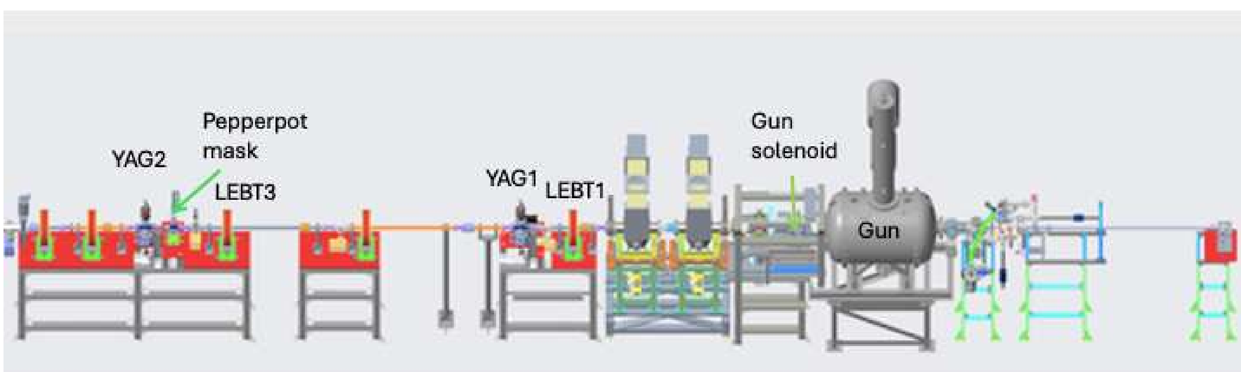

Figure 1: Low energy beamline layout. The first solenoid is placed on the exit from the gun. The other five solenoids shown in red have identical design and placed after the bunching cavities.

The accelerated beam parameters are measured in the dedicated diagnostics beamline shown in Fig. 2. The beam emittance can be measured with one of the triplet quadrupoles Q1-Q3 placed between the linac and the first dipole. The beam cross section is measured with ACC YAG profile monitor. The four quadrupoles Q1-Q4 in the diagnostics beamline provide the beam optics required for measurements.

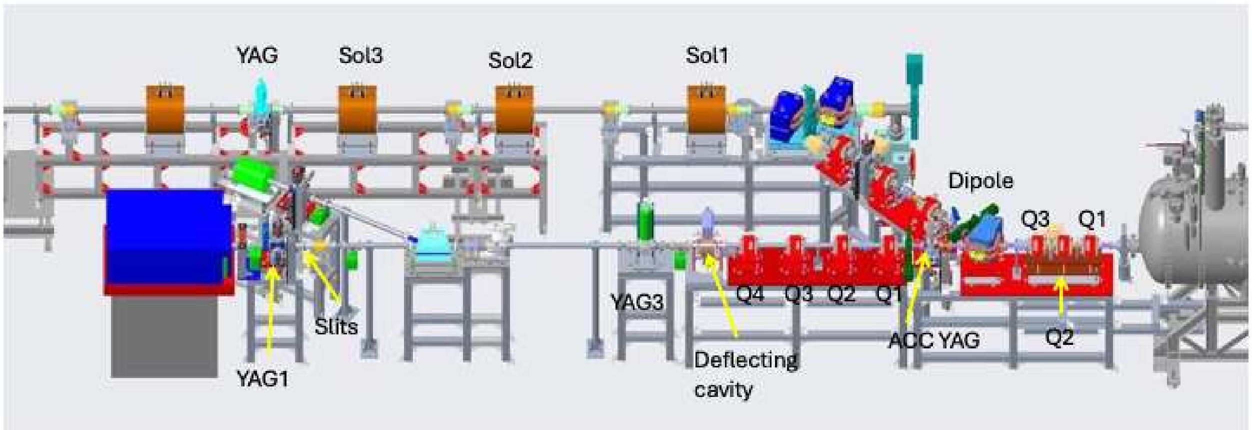

Figure 2: Layout of the CeC diagnostics line. The triplet quadrupoles after linac are used for beam function measurements. The quadrupoles Q1-Q4 are placed after the dipole in the diagnostics line.

The transverse deflecting cavity [9] tuned to 1.3 GHz provides vertical streak of the beam. The transverse beam profiles can be observed with three profile monitors. The first profile monitor YAG3 is placed before the 45-degree dipole and used for measurement of the longitudinal profile of the beam. This screen is also used for slice emittance measurement using quadrupole scan. The second profile monitor YAG1 is placed in front of the high-power dump and is preceded by two (one vertical and one horizontal) slits.

The third profile monitor is placed after the 30-degree dipole and is used for measurement of the energy slew and the slice energy spread.

In the common section there is one profile monitor after the third solenoid Sol3 which is used for verifying parameters of the electron beam interacting with hadrons.

Quadrupole Scan

Quadrupole scan is the most common way of measurement of the transverse beam parameters [10]. We treated the quadrupole as a thin lens with known focal length F (positive value for the focusing lens). The focal length was calculated from the magnetic measurements data and the beam energy. The beam is observed on the profile monitor placed at distance L from the quadrupole center. The quadrupole current is scanned in the operator defined range and the square of the beam size plotted vs. the ratio L/F. The measured dependencies are approximated with the second order polynomic fit.

$$\sigma^2(L/F) = A\left(\frac{L}{F}\right)^2 + B\frac{L}{F} + C \tag{1}$$

The beam parameters are calculated from the formulas below:

$$\begin{gathered} \varepsilon = \sqrt{(AC - B^2/4)}/L \\ \beta = A/\varepsilon \\ \alpha = \frac{2A+B}{2L\varepsilon} \end{gathered} \tag{2}$$

The application is also calculating the distance from the quadrupole to the waist and value of the β-function at the waist location. This is a convenient way to evaluate accuracy of the measurements when more then one quadrupole is used for measurement. The screenshot of the application is shown in Fig. 3.

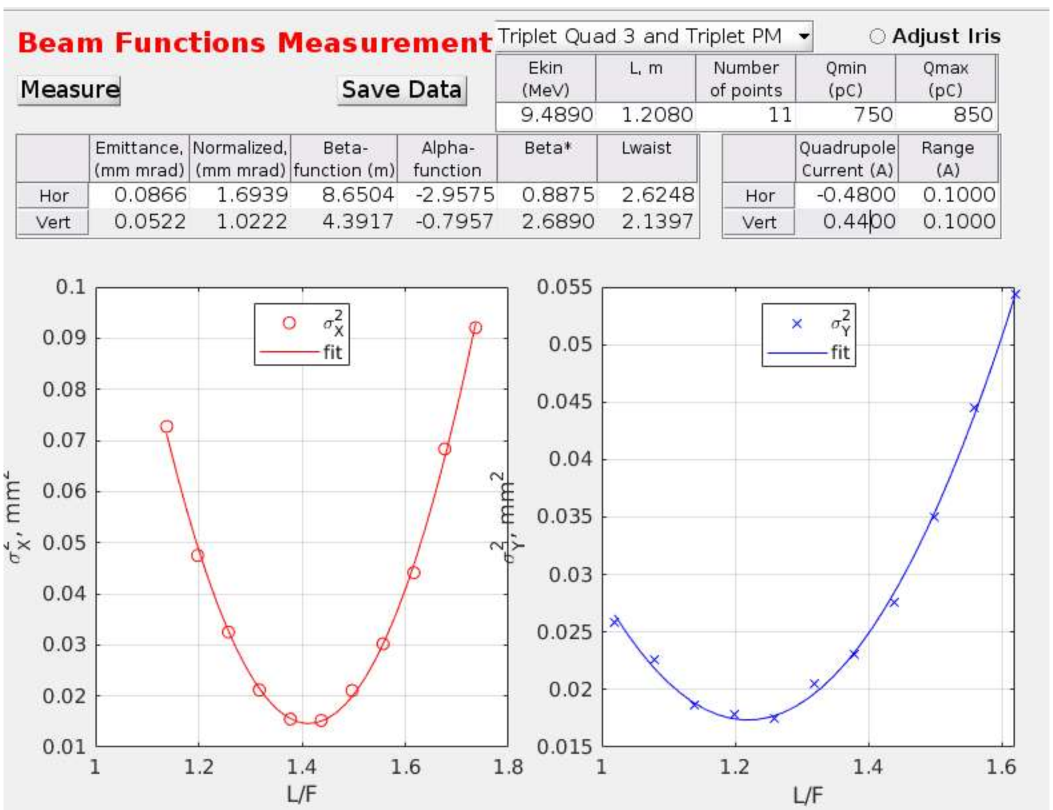

Figure 3: Screenshot of the application of the emittance measurement with quadrupole scan. Operator can choose the quadrupole/profile monitor pair, set the range of charge when the results are accepted, and define the range of the quadrupole current. By selecting the “Adjust Iris” operator will allow modification of the camera lens iris to upkeep the beam spot brightness.

Solenoid Scan

Solenoid is another focusing element which can be used for emittance measurement. The transfer matrix M_{sol} of ideal solenoid (uniform field) is

$$M_{sol} = \begin{bmatrix} \cos^2\theta & \frac{1}{g}\sin\theta\cos\theta & -\sin\theta\cos\theta & -\frac{1}{g}\sin^2\theta \\ -g\sin\theta\cos\theta & \cos^2\theta & g\sin^2\theta & -\sin\theta\cos\theta \\ \sin\theta\cos\theta & \frac{1}{g}\sin^2\theta & \cos^2\theta & \frac{1}{g}\sin\theta\cos\theta \\ -g\sin^2\theta & \sin\theta\cos\theta & -g\sin\theta\cos\theta & \cos^2\theta \end{bmatrix} \tag{3}$$

where $g = \frac{eB_{\parallel}}{2p}$ is solenoidal field strength, $\theta = gL_{eff}$ is rotation angle. Both $B_{\parallel}$ and L_{eff} are the effective values conserving the integrals of the solenoid's magnetic field and its square.

The beams without axial symmetry require a dedicated 4D analysis. In general case Twiss parametrization is not applicable and one can utilize only the measurements of the second moments of the transverse distribution $\langle x^2\rangle$, $\langle x'^2\rangle$, $\langle xx'\rangle$, $\langle y^2\rangle$, $\langle y'^2\rangle$, $\langle yy'\rangle$, $\langle xy\rangle$, $\langle xy'\rangle$, $\langle x'y\rangle$, and $\langle x'y'\rangle$ (here we assume that all the first moments are equal to zero). Profile monitor provides the three observables $\langle x^2\rangle = \sigma_x^2$, $\langle y^2\rangle = \sigma_y^2$, and $\langle xy\rangle = \sigma_{xy}$. For the N measurements we can write

$$\begin{pmatrix} \sigma_{x(1)}^2 \\ \sigma_{y(1)}^2 \\ \sigma_{xy(1)} \\ \cdots \\ \sigma_{x(N)}^2 \\ \sigma_{y(N)}^2 \\ \sigma_{xy(N)} \end{pmatrix} = \mathrm{A} \begin{pmatrix} \langle x^2\rangle \\ \langle xx'\rangle \\ \langle x'^2\rangle \\ \langle y^2\rangle \\ \langle y'^2\rangle \\ \langle yy'\rangle \\ \langle xy\rangle \\ \langle x'y'\rangle \\ \langle x'y\rangle \\ \langle xy'\rangle \end{pmatrix} \tag{4}$$

where A is $3N \times 10$ matrix formed using elements of the transfer matrix $M = M_{drift}M_{sol}$ [10]. On the left side of the Eq. 4 is columnar vector with experimental observables, and on the right side are the ten seconds moments of the beam distribution at the point of interest. For the illustration we show the dependencies of the second moments from the transfer matrix and the initial ten moments (we do not show A explicitly due to its size):

$$\sigma_x^2 = M_{11}^2\langle x^2\rangle + 2M_{11}M_{12}\langle xx'\rangle + M_{12}^2\langle x'^2\rangle + M_{13}^2\langle y^2\rangle + 2M_{13}M_{14}\langle yy'\rangle +$$

$$+M_{14}^2\langle y'^2\rangle + 2M_{11}M_{13}\langle xy\rangle + 2M_{12}M_{14}\langle x'y'\rangle + 2M_{11}M_{14}\langle xy'\rangle + 2M_{12}M_{13}\langle x'y\rangle \quad (5)$$

$$\sigma_y^2 = M_{31}^2\langle x^2\rangle + 2M_{31}M_{32}\langle xx'\rangle + M_{32}^2\langle {x'}^2\rangle + M_{33}^2\langle y^2\rangle + 2M_{33}M_{34}\langle yy'\rangle +$$

$$+M_{34}^2\langle y'^2\rangle + 2M_{31}M_{33}\langle xy\rangle + 2M_{32}M_{34}\langle x'y'\rangle + 2M_{31}M_{34}\langle xy'\rangle + 2M_{32}M_{33}\langle x'y\rangle \quad (6)$$

$$\sigma_{xy} = M_{11}M_{31}\langle x^2\rangle + (M_{11}M_{32} + M_{12}M_{31})\langle xx'\rangle + M_{12}M_{32}\langle {x'}^2\rangle + M_{13}M_{33}\langle y^2\rangle +$$

$$(M_{13}M_{34} + M_{14}M_{34})\langle yy'\rangle + M_{14}M_{34}\langle y'^2\rangle + (M_{11}M_{33} + M_{13}M_{31})\langle xy\rangle + \quad (7)$$

$$(M_{12}M_{34} + M_{14}M_{32})\langle x'y'\rangle + (M_{11}M_{34} + M_{14}M_{31})\langle xy'\rangle + (M_{12}M_{33} + M_{13}M_{32})\langle x'y\rangle$$

The second moments can be found by solving the system of linear equations when at least four measurements have been performed. However, matrix A is rank deficient. No matter how many experimental points we have the matrix rank is 9. Analysis showed that this is a fundamental feature of the system containing only solenoids and drifts. Neither the transfer matrix of a solenoid nor the transfer matrix of a drift changes the angular momentum $\langle x'y - xy'\rangle$. Addition of a quadrupole into the transport line can help to resolve these moments. We do not have any quadrupoles in the low energy beam transport, therefore in the analysis of the experimental results we assumed that $\langle x'y\rangle = \langle x'xy'\rangle$, e.g. zero angular momentum of the beam.

The screenshot of the application is shown in Fig. 4. Operator can select the solenoid, set the range of the solenoid current, and number of points. The acceptable range of bunch charges and beam energy can be set as well. Since the image brightness substantially varies, the application adjusts the camera iris. During the measurements the transfer matrix coefficients are calculated, and the values of the matrix A are filled. The experimental values of the beam image are inserted into the different matrix. After the data have been collected the system of over constrained linear equations is solved for the beam second moments. The solution minimizes the penalty function $\chi^2 = \sum\left(\left(\sigma_x/\sigma_{xfit} - 1\right)^2 + \left(\sigma_y/\sigma_{yfit} - 1\right)^2 + \left(\sigma_{xy}/\sigma_{xyfit} - 1\right)^2\right)$.

After the second moments are found, we can calculate emittances using conventional formula:

$$\varepsilon_{x,y} = \sqrt{\sigma_{x^2,y^2}^2\sigma_{x'^2,y'^2}^2 - \sigma_{xx',yy'}^2} \quad (8)$$

The script also calculates the eigen emittances [11,12] using σ-matrix S

$$S = \begin{bmatrix} \sigma_{x^2} & \sigma_{xx'} & \sigma_{xy} & \sigma_{xy'} \\ \sigma_{xx'} & \sigma_{x'^2} & \sigma_{x'y} & \sigma_{x'y'} \\ \sigma_{xy} & \sigma_{x'y} & \sigma_{y^2} & \sigma_{yy} \\ \sigma_{xy'} & \sigma_{x'y'} & \sigma_{yy} & \sigma_{y'^2} \end{bmatrix} \quad (9)$$

$$\varepsilon_{1,2} = \frac{1}{2}\sqrt{-Trace[(SJ)^2] \pm \sqrt{-Trace^2[(SJ)^2] - 16det(S)}} \tag{10}$$

where J is

$$J = \begin{bmatrix} 0 & 1 & 0 & 0 \\ -1 & 0 & 0 & 0 \\ 0 & 0 & 0 & 1 \\ 0 & 0 & -1 & 0 \end{bmatrix} \tag{11}$$

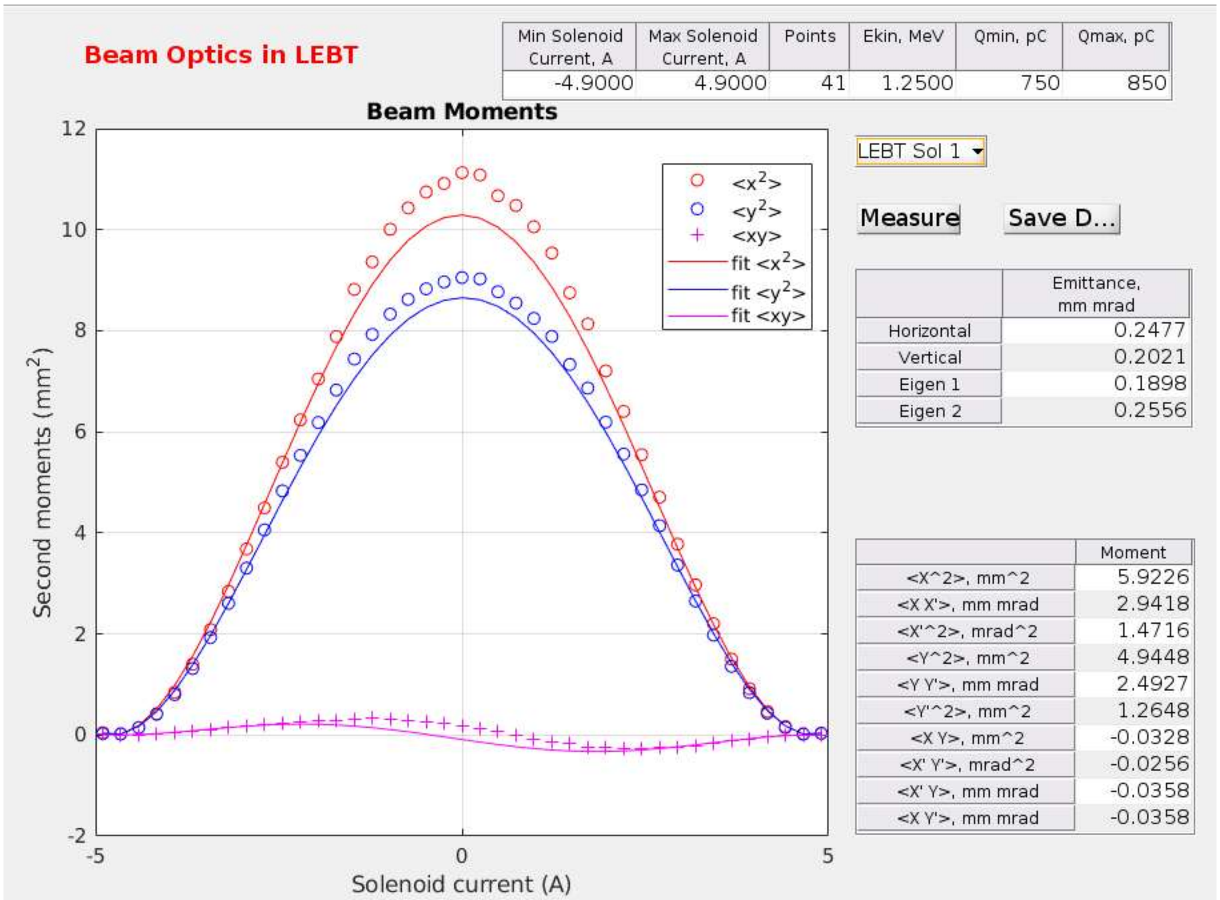

Figure 4: Screenshot of the application for the solenoid scan.

Double Solenoid Scan

Double solenoid scan was developed to suppress the rotation of the electron beam and make the measurement like the quadrupole scan. The application screenshot is shown in Fig. 5. Operator can select pair of solenoids in the common section: either the solenoids Sol2 and Sol3 or the solenoids Sol1 and Sol2. Each pair has identical solenoids with opposite direction of the magnetic field. The second order moments are calculated for each plane separately, and the emittances are calculated.

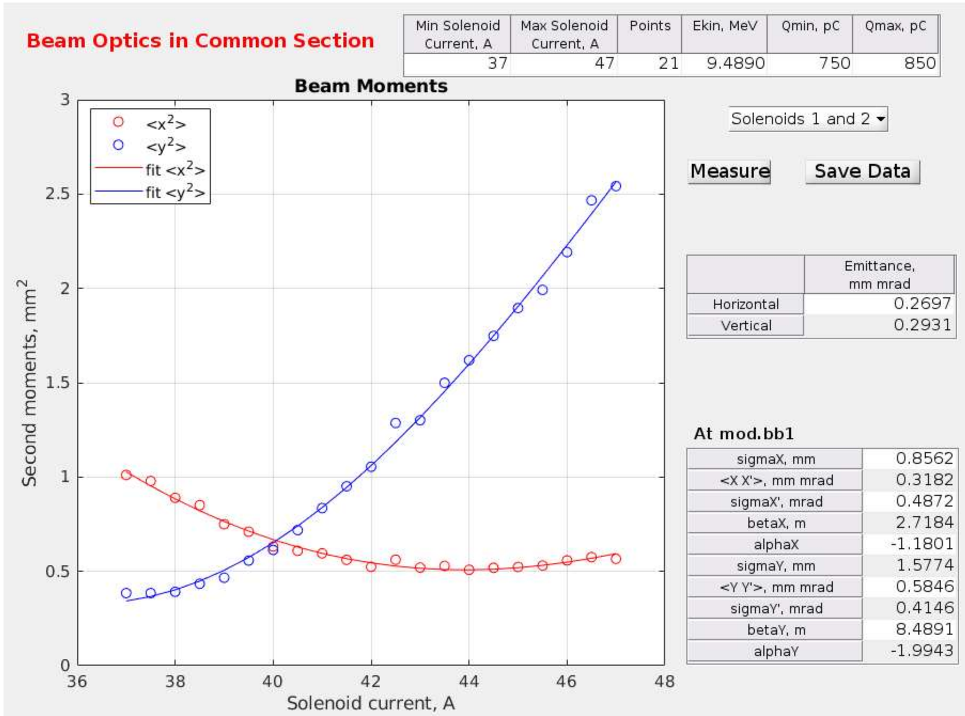

Figure 5: Screenshot of the application for the double solenoid scan.

Measurement of the Emittance with Pepper Pot

The low energy beamline has a mask with pinholes are separated by D=1 mm and forming the square pattern. Downstream of the mask at distance L=0.352 m there is the screen to observe beam. The image can be seen in Fig. 6.

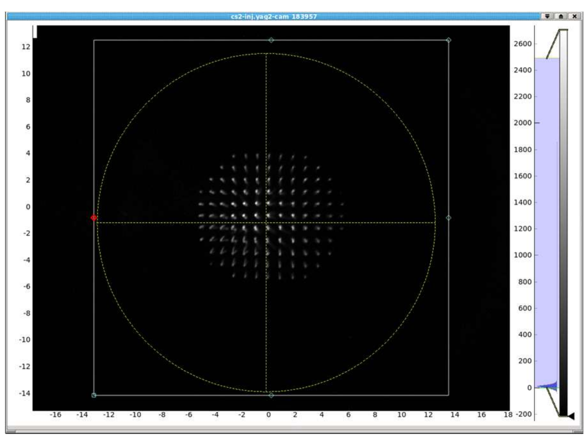

Figure 6: Image of the beam on the screen after the pepper pot.

The image of the beam passing through the mask can be processed by two applications. The Python script uses projection on the X and Y axes and handles data as the beam has passed through a set of slits. For each axis the peaks are found. There location, amplitude, and width are used for calculating beam emittances and Twiss parameters as shown in Fig. 7. The corresponding phase space is displayed in the pop-up window shown in Fig. 8.

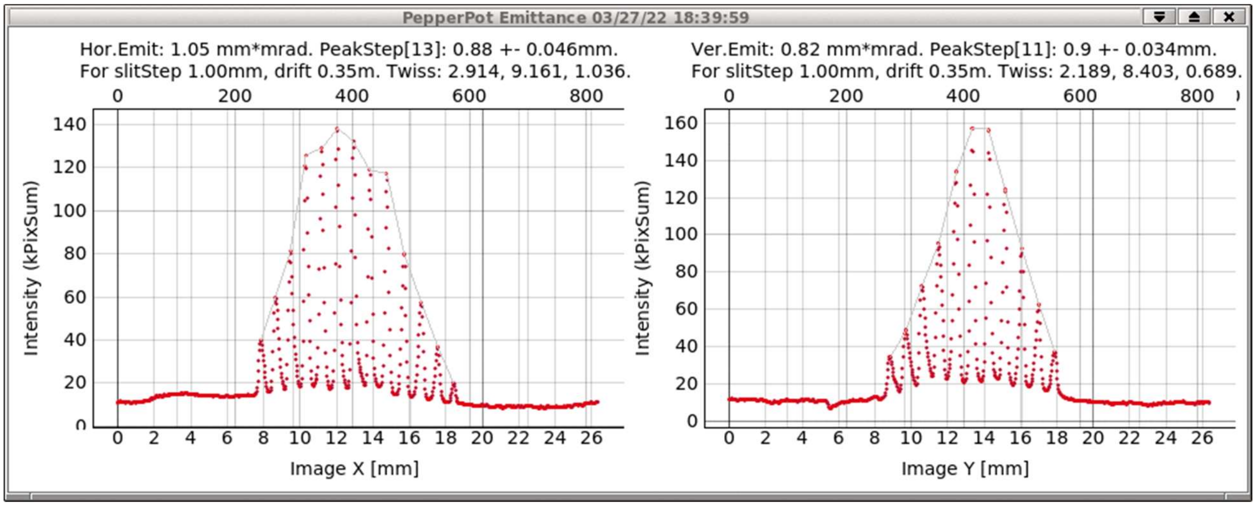

Figure 7: Screenshot of the Python application for emittance measurement using pepper pot.

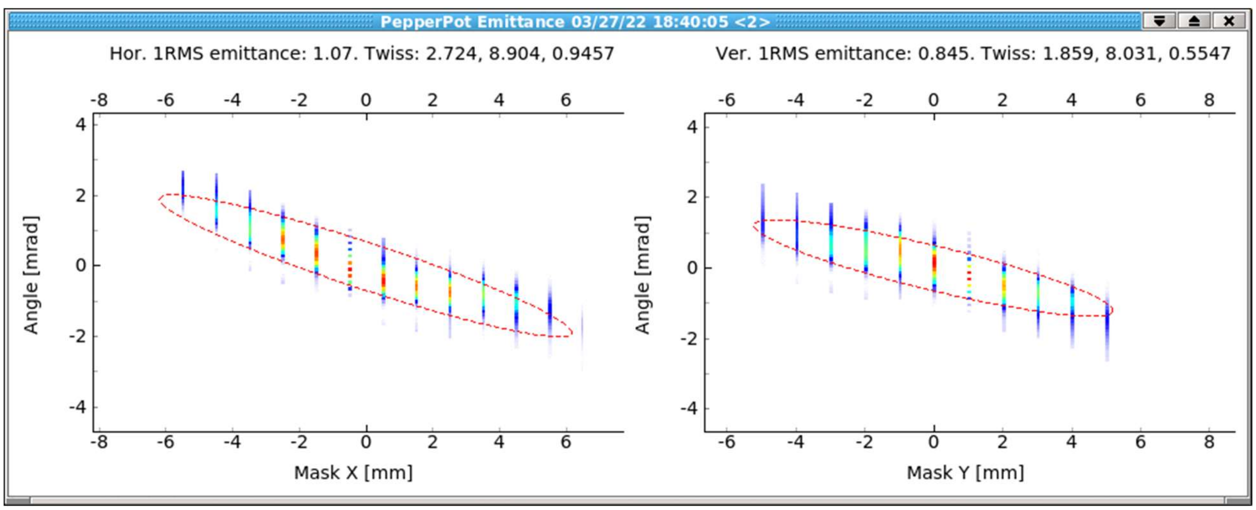

Figure 8: Reconstructed phase space from the pepper pot measurements.

The MATLAB-based application uses spot information from the image processing software in the control system. It provides data on number of detected spots N, spot intensities w_i, spot positions x_i and y_j, spot sizes σ_{xi} and σ_{yi}. To process the data the application transforms one-dimensional array into the two-dimensional. For this purpose, at first, it finds the spot closest to the center of the gravity of the beam. The spot is assigned indices (0,0). Then the spot closest to the (0,0) spot is found. The distance d between the two is used for calculations of indices for all spots:

$$\begin{aligned} i &= \mathrm{round}((x - x_{00})/d) \\ j &= \mathrm{round}((y - y_{00})/d) \end{aligned} \quad (12)$$

These indices are used as pointer for the pinhole and are used for calculation of the position of the beamlet at mask.

$$X_{ij} = D(i-1)$$
$$Y_{ij} = D(j-1) \tag{13}$$

Then the beamlet angles are calculated.

$$\alpha_{xij} = \left(x_{ij} - X_{ij}\right)/L$$
$$\alpha_{yij} = \left(y_{ij} - Y_{ij}\right)/L \tag{14}$$

Now using the spot brightness as weight of the beamlet script calculates the second moments and emittances.

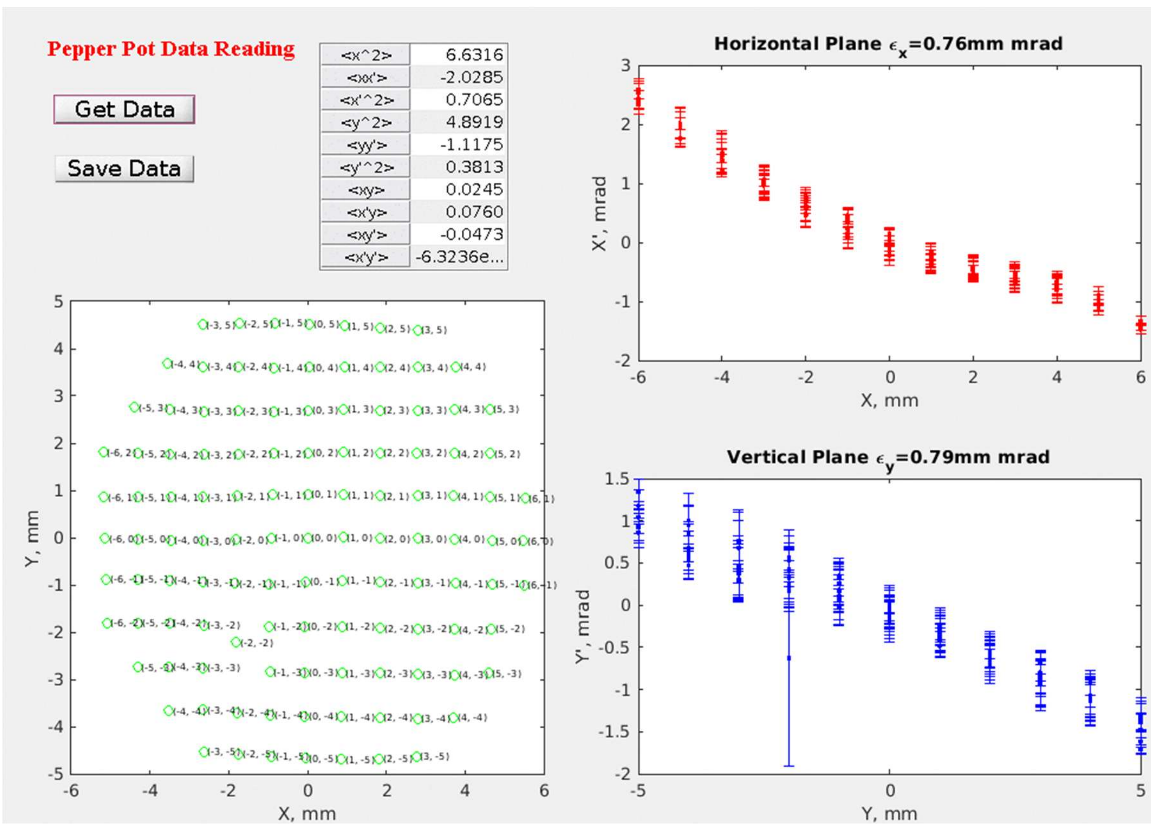

Figure 9: Screenshot of the MATLAB application for emittance measurement using pepper pot.

Slit Scan

To suppress the effects of the space charge on the emittance measurement we utilized the slits installed in the diagnostics line. The beam is moved across the slit, and image is observed on a downstream profile monitor. The angular distribution is estimated from the spatial distribution observed on the screen, and the transverse beam size at the location of the slit is found from the dependence of image intensity from the beam position on the slit.

In our experiment we utilize the fixed slits, and we are scanning the beam with the help of the calibrated trims. The calibration is performed by observing the beam motion on the screen when slits are retracted.

Beamlet intensity w_i is estimated from the image brightness. The angle α_i is found from its center of gravity on the profile monitor, and uncorrelated divergence σ_i is calculated from the beamlet width.

The emittances are calculated using conventional formula with zeroed first moments

$$\varepsilon_{slice}^2 = \langle x^2 \rangle \langle x'^2 \rangle - \langle xx' \rangle^2 \tag{15}$$

where the average values are supposed to be equal to zero. The displacement of the beam by trim is Δ_i and beamlet r.m.s. size is:

$$\langle x^2 \rangle = \sum \Delta_i^2 w_i / \sum w_i \tag{16}$$

and beam divergence is:

$$\langle x'^2 \rangle = \sum (\alpha_i^2 + \sigma_{x'i}^2) w_i / \sum w_i \tag{17}$$

Similar, the correlation term is found:

$$\langle xx' \rangle = \sum \Delta_i \alpha_i w_i / \sum w_i \tag{18}$$

The screenshot of the application for the emittance measurement with slits is shown in Fig. 10. Operator can choose the slit, set the range of the trim current and number of spots. The application displays found beam size and divergence and calculated emittance. To reduce the systematic errors the electron beam should be properly focused on the slit. Usually, the last two quadrupoles Q3 and Q4 in the diagnostics beamline are used. For the horizontal emittance Q3 is defocusing and Q4 is focusing to obtain small horizontal beam size. For the vertical emittance the Q3 is focusing and Q4 is defocusing. Usually, one focuses beam on the screen with slits being retracted and slightly increases the Q4 strength.

The lower limit for the size is defined by the slit width of 100 microns. It should not be too large either. The large beam size provides for small uncorrelated divergence, which should exceed the slit width divided by the distance to the slit.

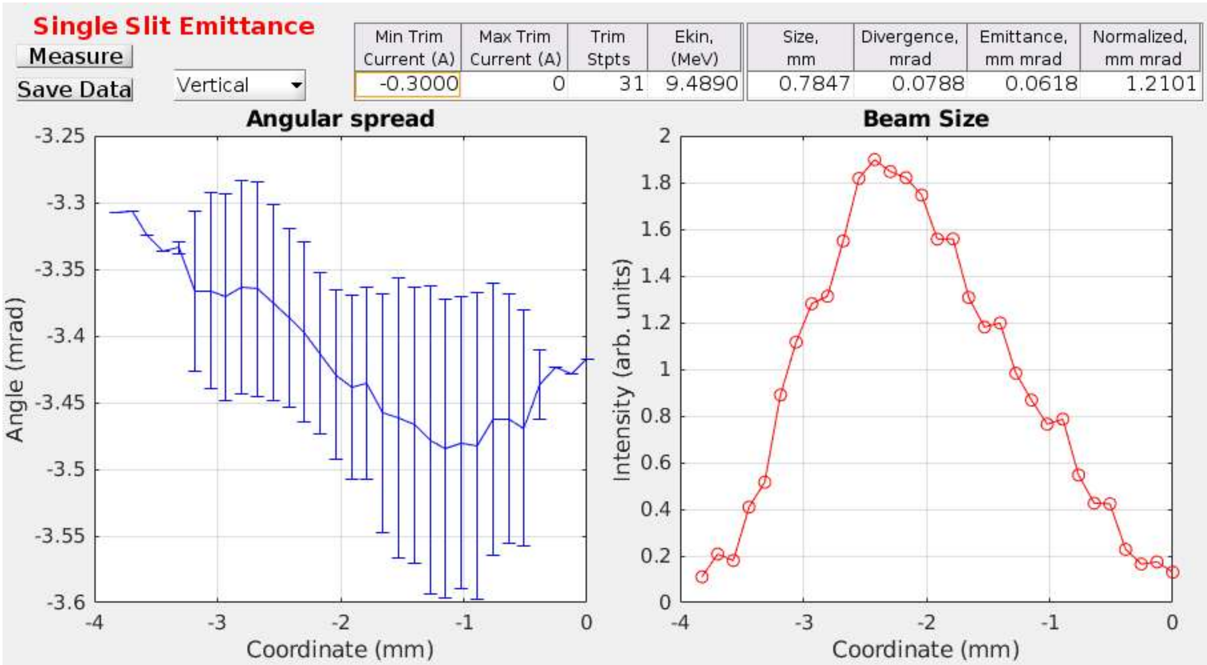

Figure 10: Screenshot of the application for the beam emittance measurement with slits.

Slice Emittance Measurement with Slit

The slice emittance is measured with help of the deflecting cavity. Since the beam is spread vertically, only horizontal slice emittance can be measured. The measurement set-up includes centering of the beam with the quadrupole Q4, phasing of the deflecting cavity, and centering of the beam on the profile monitor. The centering is needed since selection of the slice is realized with change of the region of interest. It is modified to a narrow horizontal band. The beam focusing is performed in the manner previously described for the slit scan. The scan of the beam across the slit is performed with the calibrated horizontal trim.

Time scan is performed by changing the deflecting cavity phase. In such approach. calibration of the deflecting cavity is not required. Beamlet intensity w_i is estimated from the image brightness inside of the region of interest. The beamlet angle α_i is found from its center of gravity of the image spot on the profile monitor and uncorrelated divergence $\sigma_{x'i}$ from the beamlet width. The measured beam size is corrected for the final resolution of the system defined by point spread function of the optical system and slit width. The result of the scan is shown in Fig. 11.

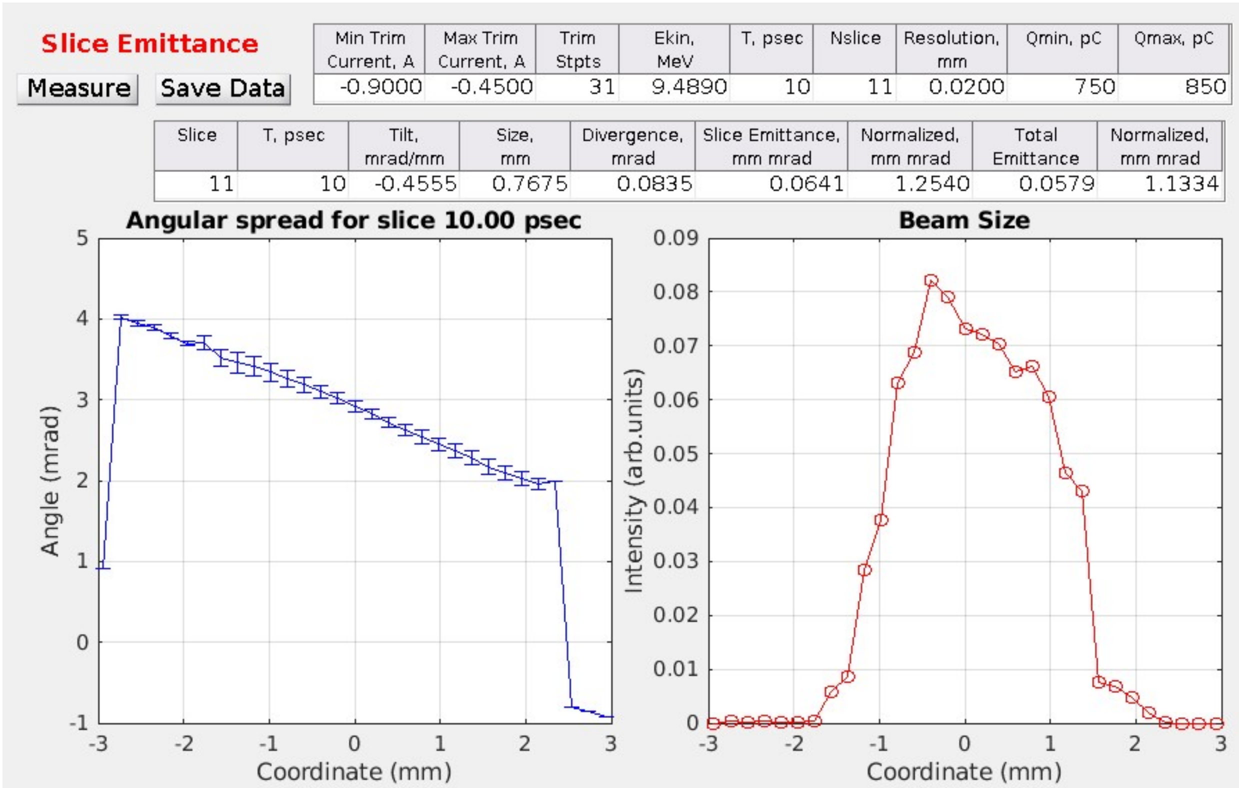

Figure 11: Snapshot of the application for the slice emittance measurement.

The slice is defined by region of interest on the profile monitor. The location of the ROI is fixed during the measurement, and temporal scan is done by changing the phase of deflecting cavity. Such approach does not require knowledge of the cavity voltage and calibration of deflecting angle. The calibration, however, is used for setting the vertical size of ROI.

The emittance of the whole bunch is calculated from the slices data. The weight of each slice is sum of the beamlet intensities. The position and angle of each slice is used with weighted average. Uncorrelated angular divergence is used from the slice data. Emittance calculation is based on equations (15-18). The emittance of the whole beam is displayed upon completion of the last slice measurement.

References

[1] I. Pinayev et al., “Performance of CeC PoP Accelerator,” in Proc. 10th Int. Particle Accelerator Conf. (IPAC’19), Melbourne, Australia, May 2019, pp. 559-561. doi:10.18429/JACoW-IPAC2019-MOPMP050

[2] Min Zhang, “Emittance Formula for Slits and Pepper-pot Measurement”, Fermilab Technical Note FERMILAB-TM-19, 1996.

[3] H. R. Kremers, J. P. M. Beijers, and S. Brandenburg, “A pepper-pot emittance meter for low-energy heavy-ion beams”, Rev. Sci. Instrum. 84, 025117 (2013); https://doi.org/10.1063/1.4793375

[4] R. Niemczyk et al., “Slit-based Slice Emittance Measurements Optimization at PITZ”, in Proc. IBIC’19, Malmo, Sweden, Sep. 2019, pp. 318-321. doi:10.18429/JACoW-IBIC2019-TUPP013

[5] M. Roehrs, C. Gerth, M. Huening, H. Schlarb, “Slice Emittance Measurements at FLASH”, in Proc. 10th European Particle Accelerator Conf. (EPAC’06), Edinburgh, Scotland, UK, June 2006, pp. 77-79.

[6] J. Rudolph, M. Abo-Bakr, T. Kamps, J. Teichert, “Slice Emittance Measurement at ALBE/SRF Injector”, in Proc. DIPAC’11, Hamburg, Germany, May 2011, pp. 416-418.

[7] K. Shih, G. Wang, J. Ma, I. Pinayev, Y. Jing, V. N. Litvinenko, I. Petrushina, “Demonstration of time-resolved diagnostic in coherent electron cooling pop experiment”, in. Proc. IPAC2024, Nashville, USA, doi:10.18429/JACoW-IPAC2024-WEPG11.

[8] T.A. Miller et al., “Overview of Beam Instrumentation and Commissioning Results from the Coherent Electron Cooling Experiment at BNL”, in Proc. IBIC'18, Shanghai, China, Sep. 2018, pp. 43-47. doi:10.18429/JACoW-IBIC2018-MOPA09

[9] S.A. Belomestnykh, V.D. Shemelin, K.W. Smolenski, V. Veshcherevich, “Deflecting Cavity for Beam Diagnostics in ERL Injector”, in Proc. 22nd Particle Accelerator Conf. (PAC’07). Albuquerque, New Mexico, USA, June 25-29, 2007, pp.2331-2333.

[10] M.G. Minty and F. Zimmermann, Measurement and Control of Charged Particle Beams, Springer, 2003.

[11] C. Xiao, X.N. Du, L. Groening, H. Leibrock, M. Maier, and P. Rottländer, Single-knob beam line for transverse emittance partitioning, PR-STAB, **16**, 044201 (2013), doi:10.1103/PhysRevSTAB.16.044201.

[12] C. Xiao, X.N. Du, L. Groening, and M. Maier, Refining the evaluation of eigen emittances measured by the dedicated four-dimensional emittance scanner ROSE, Nuclear Inst. and Methods in Physics Research, A 964 (2020) 163828.